© 2019. Published by The Company of Biologists Ltd | Journal of Experimental Biology (2019) 222, jeb193573. doi:10.1242/jeb.193573

RESEARCH ARTICLE

Skeletal kinematics of the hyoid arch in the suction-feeding shark *Chiloscyllium plagiosum*

Bradley Scott[1,2,*], Cheryl A. D. Wilga[1,3] and Elizabeth L. Brainerd[4]

ABSTRACT

White-spotted bamboo sharks, *Chiloscyllium plagiosum*, generate strong suction-feeding pressures that rival the highest levels measured in ray-finned fishes. However, the hyostylic jaw suspension of these sharks is fundamentally different from the actinopterygian mechanism, including more mobile hyomandibulae, with the jaws and ceratohyal suspended from the hyomandibulae. Prior studies have proposed skeletal kinematics during feeding in orectolobid sharks from indirect measurements. Here, we tested these hypotheses using XROMM to measure cartilage motions directly. In agreement with prior hypotheses, we found extremely large retraction and depression of the ceratohyal, facilitated by large protraction and depression of the hyomandibula. Somewhat unexpectedly, XROMM also showed tremendous long-axis rotation (LAR) of both the ceratohyal and hyomandibula. This LAR likely increases the range of motion for the hyoid arch by keeping the elements properly articulated through their large arcs of motion. XROMM also confirmed that upper jaw protraction occurs before peak gape, similarly to actinopterygian suction feeders, but different from most other sharks in which jaw protrusion serves primarily to close the mouth. Early jaw protraction results from decoupling the rotations of the hyomandibula, with much of protraction occurring before peak gape with the other rotations lagging behind. In addition, the magnitudes of retraction and protraction of the hyoid elements are independent of the magnitude of depression, varying the shape of the mouth among feeding strikes. Hence, the large variation in suction-feeding behavior and performance may contribute to the wide dietary breadth of bamboo sharks.

KEY WORDS: Bamboo shark, Biomechanics, XROMM, Hyomandibula, Ceratohyal

INTRODUCTION

High-performance suction feeding has evolved multiple times within elasmobranch and ray-finned fishes (Wilga, 2008; Wainwright et al., 2015). Bamboo sharks generate very strong suction pressure within a very short time frame (down to −99 kPa in as little as 45 ms) and are thought to use power amplification to achieve high suction powers (Wilga et al., 2007; Wilga and Sanford, 2008; Ramsay and Wilga, 2017). In addition to extraordinary performance, suction feeding in white-spotted bamboo sharks shows broad variation in peak pressure (mean coefficient of variation, CV=1.9) and kinematics (CV=0.74), even when feeding on a single prey type (Wilga et al., 2012). Hence, suction feeding in white-spotted bamboo sharks is both high performance, defined here as the potential for fast and strong suction pressure, and non-stereotyped, defined as high variability within a single prey type (Wainwright et al., 2008).

Prior studies have used high-speed video, specimen manipulation and sonomicrometry to infer the skeletal kinematics underlying suction performance and variability in orectolobiform sharks, including white-spotted bamboo sharks (Wu, 1994; Wilga and Sanford, 2008; Ramsay, 2012; Ramsay and Wilga, 2017). In this study, we use X-ray reconstruction of moving morphology (XROMM) to test hypotheses for the 3D motions of the hyoid arch from these prior studies. The hyoid arch is hidden from view by thick skin and musculature in sharks and rays, making XROMM necessary to quantify the complex motions of the hyoid arch in relation to the chondrocranium and oral jaws.

Jaw suspension is hyostylic in bamboo sharks, with the hyomandibula suspending both Meckel's cartilage and the ceratohyal (Fig. 1). The palatoquadrate articulates with Meckel's cartilage and is also suspended by ligaments from the chondrocranium. During suction feeding, retraction of the ceratohyal–basihyal complex is thought to induce anterior protraction and depression of the hyomandibula (Wu, 1994; Wilga and Sanford, 2008; Ramsay and Wilga, 2017). The long axis of the hyomandibula is oriented mediolaterally in bamboo sharks at rest (Fig. 1A,C), such that depression increases the vertical depth of the buccal cavity, but also causes a decrease in mediolateral width (Fig. 1D).

Hence, although hyomandibular depression contributes to suction expansion, the associated decrease in mediolateral width of the buccal cavity is thought to decrease suction performance in elasmobranchs with mediolaterally oriented hyomandibulae (Wilga, 2008; Wilga and Sanford, 2008). By contrast, the hyomandibula in ray-finned fishes is vertically oriented and integrated into the suspensorium complex. This vertical orientation combined with cranial linkage systems makes it possible for actinopterygians to expand the buccal cavity laterally as well as dorsoventrally for suction feeding (van Dobben, 1937; Tchernavin, 1948; Alexander, 1967; Liem, 1967; Osse, 1969; Wilga, 2008; Olsen et al., 2017). Yet, despite the putative constraint in their hyoid arch motions, the suction performance of white-spotted bamboo sharks exceeds that of most ray-finned fishes. How do these sharks achieve such high suction performance?

High suction performance may result from exceptionally high magnitude rotations of the hyoid arch, as has been hypothesized from external view video, sonomicrometry and manipulations of dead specimens (Wu, 1994; Wilga and Sanford, 2008; Ramsay and Wilga, 2017). Drawings from manipulations suggest about 45 deg of rotation for the hyomandibula and more than 90 deg of ceratohyal rotation (Fig. 1B). These are extreme rotations relative to suspensorial and ceratohyal rotations visualized with XROMM in ray-finned fishes (Camp et al., 2015, 2018; Camp and Brainerd, 2015), although hyoid

[1]Department of Biological Sciences, University of Rhode Island, 120 Flagg Road, Kingston, RI 02881, USA. [2]Department of Animal Biology, University of Illinois Urbana-Champaign, Victor E. Shelford Vivarium, Champaign, IL 61820, USA. [3]Department of Biological Sciences, University of Alaska Anchorage 3101 Science Circle, Anchorage, AK 99508, USA. [4]Department of Ecology and Evolutionary Biology, Brown University, Providence, RI 02912, USA.

*Author for correspondence (brscott2@illinois.edu)

B.S., 0000-0002-0599-1152; E.L.B., 0000-0003-0375-8231

Received 1 October 2018; Accepted 8 January 2019

Journal of Experimental Biology (2019) 222, jeb193573. doi:10.1242/jeb.193573

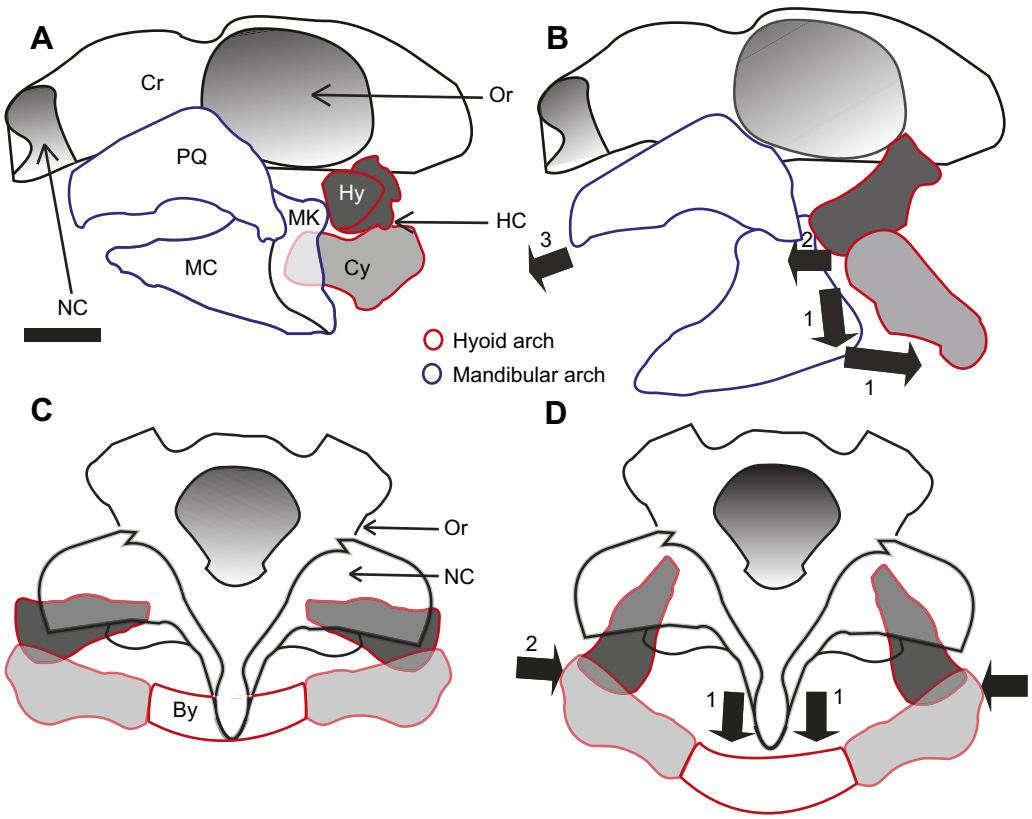

Fig. 1. Hypothetical motions of the hyoid arch, including the hyomandibula and ceratohyal of orectolobiform sharks during suction feeding. The hyomandibula (dark gray) and ceratohyal (light gray) are not visible externally, so hypothetical motions have been inferred from *ex vivo* manipulations, sonomicrometry and changes in head shape from external video (Wu, 1994; Wilga, 2008; Wilga and Sanford, 2008). (A) Cartilaginous elements of the head at rest, in left lateral view. (B) Cartilaginous elements at maximum gape and hyoid depression. (C,D) Anterior view of the cranium and hyoid elements in resting position (C) and depressed position (D). The distal end of the ceratohyal moves ventrally and caudally (black arrows 1) as the proximal end of the ceratohyal and distal end of the hyomandibula move rostrally and medially (black arrows 2) and contribute to protrusion of the palatoquadrate (black arrow 3). By, basihyal; Cr, cranium; Cy, ceratohyal; Hy, hyomandibula; HC, hyomandibuloceratohyal joint; MC, Meckel's cartilage; MK, knob on Meckel's cartilage that articulates with hyomandibula at the hyomandibulomandibular joint; NC, nasal capsule; Or, orbit; PQ, palatoquadrate. Scale bar: 10 mm.

rotation in some groups, such as Sygnathiformes, can be as large (Van Wassenbergh et al., 2008, 2013). Here, we use XROMM to determine whether such extreme hyoid rotations actually occur *in vivo* in white-spotted bamboo sharks.

As noted above, depression of the hyomandibulae may decrease mediolateral width of the buccal cavity (Fig. 1D) and decrease suction performance. However, sonomicrometry has shown that the increase in vertical depth of the buccal cavity begins before a decrease in lateral width, and most of the decrease in lateral width occurs after peak gape (Wilga and Sanford, 2008). This delay in medial compression may mitigate its negative effects on suction pressure generation, but how is the delay achieved? With XROMM we can measure separate degrees of rotation of the hyomandibula to determine whether medial and ventral motion are decoupled to delay medial compression and increase suction performance.

In ray-finned fishes, jaw protrusion increases suction feeding performance by moving the mouth aperture and suction flow field closer to the prey (Wainwright et al., 2015), but in most elasmobranchs, peak jaw protrusion occurs after peak gape and contributes to jaw closing rather than to suction performance (Wilga et al., 2007). In bamboo sharks, however, the palatoquadrate is thought to move rostrally before peak gape, potentially contributing to suction performance, and then rotates ventrally to help close the gape (Wu, 1994; Wilga and Sanford, 2008). Jaw protrusion is driven by motions of the hyomandibula, and rotation of the hyomandibula is hypothesized to produce both protraction and depression of its distal end (Fig. 1B). Meckel's cartilage articulates with the distal hyomandibula, and the palatoquadrate articulates with Meckel's cartilage, so rotation of the hyomandibula is expected to cause protraction and depression of the upper and lower jaws (Fig. 1B). Decoupled rotations of the hyomandibula could produce rostral and then ventral jaw protrusion if the hyomandibula protracts before it depresses. Here, we use XROMM to visualize the jaws throughout the strike and relate rotation of the hyomandibula to jaw protrusion.

Lastly, as noted above, suction feeding performance in white-spotted bamboo sharks is also highly variable (non-stereotyped). Decoupling hyoid arch motions could be responsible for the wide variation in suction performance among feeding strikes. We test the hypothesis that decoupling of horizontal and vertical hyoid arch motions occurs by determining whether retraction and protraction of the ceratohyal and hyomandibular cartilages are independent of their respective depression during suction feeding. If decoupling occurs, then the time and magnitude of horizontal motions will vary independently of vertical motions, enabling bamboo sharks to actively vary the shape of the oral cavity.

MATERIALS AND METHODS

Animals and implantation procedure

Three individuals of *Chiloscyllium plagiosum* (Bennett 1830) of similar size (78.6 cm, 79.2 cm, 85 cm; chondrocrania 6.47 cm,

Journal of Experimental Biology (2019) 222, jeb193573. doi:10.1242/jeb.193573

6.35 cm, 6.58 cm long, respectively) were used. The sharks were anesthetized with 0.033 g l^{-1} tricaine methanesulfonate (MS-222) in a recirculating fish anesthesia system (Wilga and Sanford, 2008). Three conical tungsten carbide markers (Kambic et al., 2014) were implanted in each of the cranium, palatoquadrate, Meckel's, hyomandibula and ceratohyal cartilages on the left side of the head (Fig. 2). All experimental procedures were approved by Institutional Animal Care and Use Committees of Brown University and the University of Rhode Island. All sharks recovered to feed normally following implantation.

CT scans

The sharks were CT scanned to determine marker positions and to create mesh models of the chondrocranium and skeletal elements in the mandibular and hyoid arches. Sharks were anesthetized with 0.033 g l^{-1} tricaine methanesulfonate (MS-222) in seawater. Individuals were then placed in a FIDEX CT scanner (Animage) at Brown University and scanned at an isotropic resolution of 0.185 mm. CT image series were compiled and reconstructed using Osirix (Pixmeo, Geneva, Switzerland). Three-dimensional surface meshes of the cranial, Meckel's, palatoquadrate, hyomandibula and ceratohyal cartilages with implanted markers were exported to Maya computer animation software (2015; Autodesk). The centroid of the vertices of each marker was calculated using the vAvg tool in the XROMM MayaTools (bitbucket.org/xromm/xromm_mayatools). Centroids of markers are exported from Maya as CT coordinates (CTex MayaTool).

Video data collection

Feeding trials were performed at the W. M. Keck Foundation XROMM Facility at Brown University. Food was withheld for 1 week prior to data collection. Individuals were fed pieces of either squid or herring for each trial, cut to approximately 50% of gape width. Feeding trials were recorded by a pair of Phantom v10 high-speed video cameras (Vision Research), each with a linked X-ray emitter and fluoroscopic image intensifier (Imaging Systems and Service). The pair of fluoroscopes recorded the motion of implanted markers at 320 or 330 Hz, with X-ray energies of 110 or 120 kV and 100 mA. Video data were managed during the study using the XMAPortal data management system and are now archived on xmaportal.org with their essential metadata in accordance with best practices for video data management in organismal biology (Brainerd et al., 2017).

For marker-based XROMM animation, we followed previously published methods (Brainerd et al., 2010; Knörlein et al., 2016). Marker position was tracked for both cameras across all trials with XMALab motion analysis open-source software (bitbucket.org/xromm/xmalab). CT coordinates were imported into XMALab and assigned to the appropriate markers. Based on the translation of each marker in an element, the displacement and rotation of the element was calculated in XMALab and exported assuming the element was a rigid body (i.e. there was no strain). Rigid-body transformations exported from XMALab were then imported into Maya and applied to the meshes of elements rendered from the CT scans (XROMM MayaTool script 'imp').

Rotation analysis using joint coordinate systems

Joint coordinate systems (JCSs; Brainerd et al., 2010; Gidmark et al., 2012; Kambic et al., 2014) were used to calculate the rotations of skeletal elements. JCSs quantify the relative motion between two rigid bodies, in this case between the chondrocranium and the hyomandibula, and between the chondrocranium and the ceratohyal (Fig. 3). We used the jAx tool in XROMM MayaTools to output JCS data as Euler angles with rotation order set as *z*-*y*-*x*. To set the JCSs, we aligned the *z*-axis to measure the largest expected rotation, which was depression–elevation for both the hyomandibula and ceratohyal, with depression negative. Then, we set the *x*-axis along the long axes of both elements to capture long-axis rotation (LAR). In an Euler angle system, the *y*-axis is a floating axis that remains orthogonal to *z* and *x*. The *y*-axis here measured protraction and retraction of the elements, with protraction positive and retraction negative (Fig. 3).

For each element, the timing of peak rotation in milliseconds relative to peak gape, and the magnitude of rotation in degrees about all three axes at the time of peak gape and the overall maximum rotation magnitudes were measured. Four trials were analyzed for each individual for a total of 12 feeding trials.

Displacement analysis using an anatomical coordinate system

An anatomical coordinate system (ACS) was aligned with the major axes of the chondrocranium and used to measure displacement

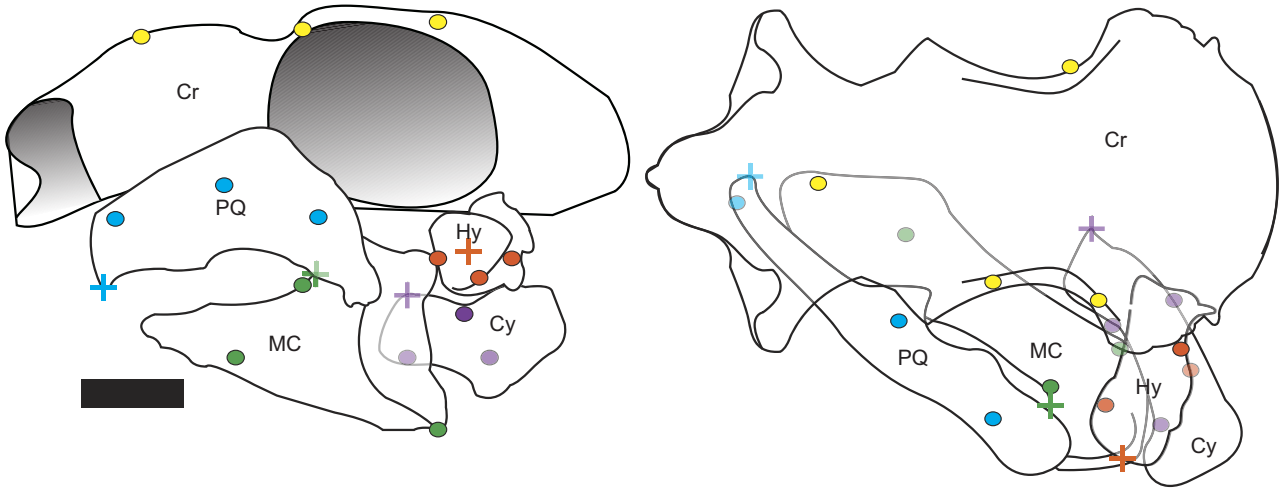

Fig. 2. Positions of implanted markers in lateral and dorsal views. Lateral view (left) and dorsal view (right); anterior is to the left of each image. Marker colors differ by cartilage element. Positions shown here are for shark Bam03, with markers placed in approximately the same position in other individuals. Crosses denote the position of the landmarks used to estimate displacement of the distal end of the hyomandibula (orange), ceratohyal (purple), jaw joint (green) and upper jaw (blue) relative to the cranium. Cr, cranium; Cy, ceratohyal; Hy, hyomandibula; MC, Meckel's cartilage; PQ, palatoquadrate. Scale bar: 10 mm.

Journal of Experimental Biology (2019) 222, jeb193573. doi:10.1242/jeb.193573

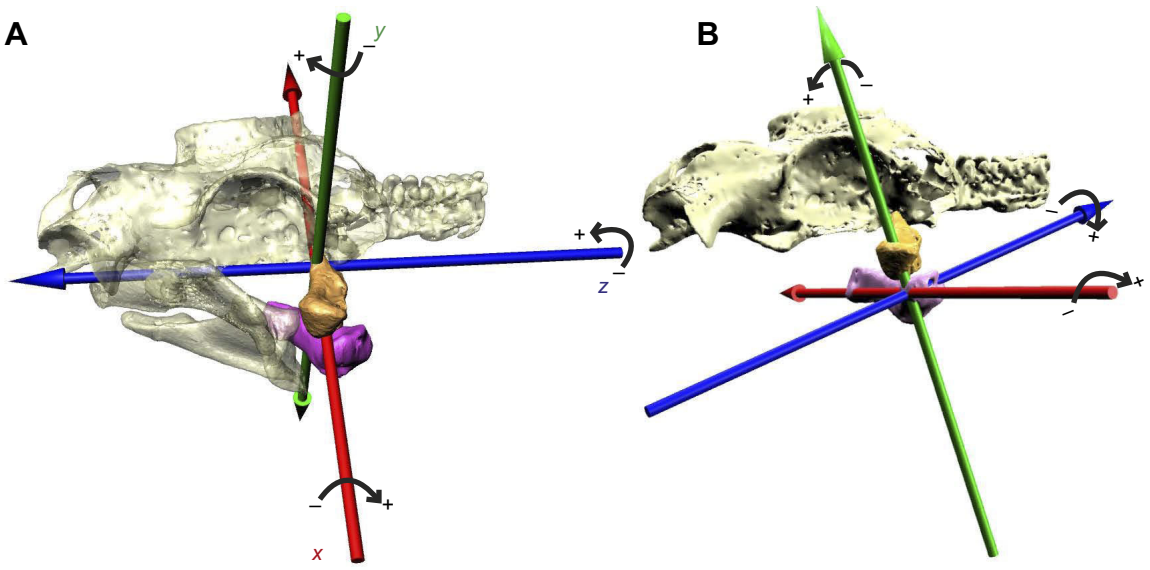

Fig. 3. Orientations of the joint coordinate systems (JCSs) for the hyomandibula and ceratohyal. (A) JCS for measuring motion of the hyomandibula (orange) relative to the chondrocranium (gold). (B) JCS for measuring motion of the ceratohyal (purple) relative to the chondrocranium (gold). For both JCSs, negative rotation about the *z*-axis is depression and positive is elevation; rotation about the *y*-axis is protraction (positive) and retraction (negative); rotation about the *x*-axis is long-axis rotation (LAR).

(Brainerd et al., 2010; Gidmark et al., 2012) of landmarks placed at the distal ends of the left hyomandibula and left ceratohyal, at the medial quadratomandibular joint facet on the left palatoquadrate, and at the rostral tip of the left palatoquadrate. Displacements of these landmarks were recorded relative to the ACS aligned with the chondrocranium, with the *x*-axis oriented mediolaterally with positive to the right, the *y*-axis oriented rostrocaudally with rostral positive, and the *z*-axis oriented dorsoventrally with dorsal positive. This ACS orientation measures: dorsal and ventral translation of the landmarks as positive and negative *x*-axis displacement, respectively; rostral and caudal translation as positive and negative *y*-axis displacement, respectively; and medial and lateral translation as positive and negative *x*-axis displacement, respectively.

Precision and accuracy of marker tracking and rigid body motion

To estimate the precision of marker tracking, we calculated the mean of mean standard deviations of marker-to-marker distance pairs for markers within each rigid body (Brainerd et al., 2010; Knörlein et al., 2016). We selected one representative trial per individual (1800–2200 frames per trial) with five rigid bodies per trial, yielding a total of 60 s.d. The result was a grand mean of mean s.d. of 0.12±0.016 mm (±s.e.m., n=60). The worst distance s.d. was 0.54 mm and the best was 0.02 mm. A large distance s.d. within a rigid body can reflect lack of rigidity of the element as well as noise in marker tracking. To test for non-rigidity, we calculated mean s.d. for each rigid body in all three individuals. The ceratohyal and hyomandibula in Bam02 and Bam04 showed slightly higher values (0.20–0.23 mm) than the overall mean, as did the Meckel's cartilage in Bam02 (0.28 mm). All cartilages in Bam03 showed low s.d. of <0.07 mm.

To estimate the precision of Euler angles and translations from JCSs, we implanted markers in the cranium and Meckel's cartilage of the head of a bamboo shark cadaver and froze it solid. We placed the frozen head in water, oscillated it at roughly the frequency and amplitude of the motions during suction feeding and recorded using the same X-ray settings as the feeding data. We CT scanned the head, made mesh models and produced an XROMM animation of two trials. We placed a JCS with the *x*-axis measuring LAR, *y*-axis protraction–retraction and *z*-axis depression–elevation (similar to hyoid JCSs). All rotations and translations in a frozen head are expected to be zero, so the s.d. of JCS outputs are a good measure of JCS precision (Menegaz et al., 2015). The Meckel's cartilage had four markers implanted with three widely spread (>15 mm apart) and one just 7 mm from another. With all four jaw markers, the errors were very small: less than 0.2 mm for translations and 0.3 deg for rotations. To mimic our three markers in the rod-like hyomandibula and ceratohyal, we removed one of the lower jaw markers from the dataset and left two markers that were just 7 mm apart and one about 15 mm from those two along the long axis of the element. In this case, as expected, the long-axis rotation (LAR) was noisier, with s.d. of 0.55 and 0.77 deg in the two trials. The other rotations were less than 0.4 deg s.d. and all translations had mean s.d. less than 0.2 mm.

Regression

Standardized major axis regressions (also known as reduced major axis regression; Smith, 2009) were used to compare ceratohyal LAR or retraction (caudal rotation) with depression (ventral rotation) of the ceratohyal at the time of peak gape, as well as at peak motion. The same comparisons were made for the hyomandibula. Rotation of the elements was measured for both *x*- and *y*-axes, therefore natural variation across both axes is expected to be similar. Since no causal relationship is being explored and variation is expected to be symmetrical, a standardized major axis regression was chosen for comparison (Warton et al., 2006; Smith, 2009). Analyses were carried out using the smatr package in R (www.rdocumentation.org/packages/smatr/). Only nine trials showed distinct positive LAR of the ceratohyal during the compressive phase, one of these peaking at less than zero degrees of positive rotation. Trials with negative LAR only were set at a magnitude of zero for regression analysis.

Three of the trials for one individual exhibited a greatly reduced positive LAR of the ceratohyal (see Discussion). Two *post hoc* single-tailed *t*-tests adjusted for heteroscedasticity (Welch, 1947) with a Bonferroni adjusted α=0.025 were used to determine whether

Journal of Experimental Biology (2019) 222, jeb193573. doi:10.1242/jeb.193573

an absence of positive LAR of the ceratohyal in three trials for Bam04 reduced depression of the ceratohyal. Another trial for Bam03 is excluded from the *t*-tests because a positive peak during the compressive phase did not exceed the resting position.

RESULTS

Bamboo sharks captured food using inertial suction in all trials and transported the food toward the back of the mouth in a single motion in 11 of the 12 trials. In one trial, prey was sucked to the mouth, grasped between the teeth, and then transported in a second motion. Very little cranial elevation was observed during these strikes (see also Camp et al., 2017).

Feeding began with mouth opening by depression of the Meckel's cartilage (Fig. 4, between −100 and 0 ms). As the Meckel's cartilage depressed and gape increased, the ceratohyal began to retract and depress, and the hyomandibula began to rotate such that the distal end depressed ventrally and protruded rostrally (most clear in Fig. 4B, between −22 and 0 ms). By the time of peak gape (Fig. 4, 0 ms), the palatoquadrate showed substantial rostral protrusion and the hyomandibula and ceratohyal had not yet reached

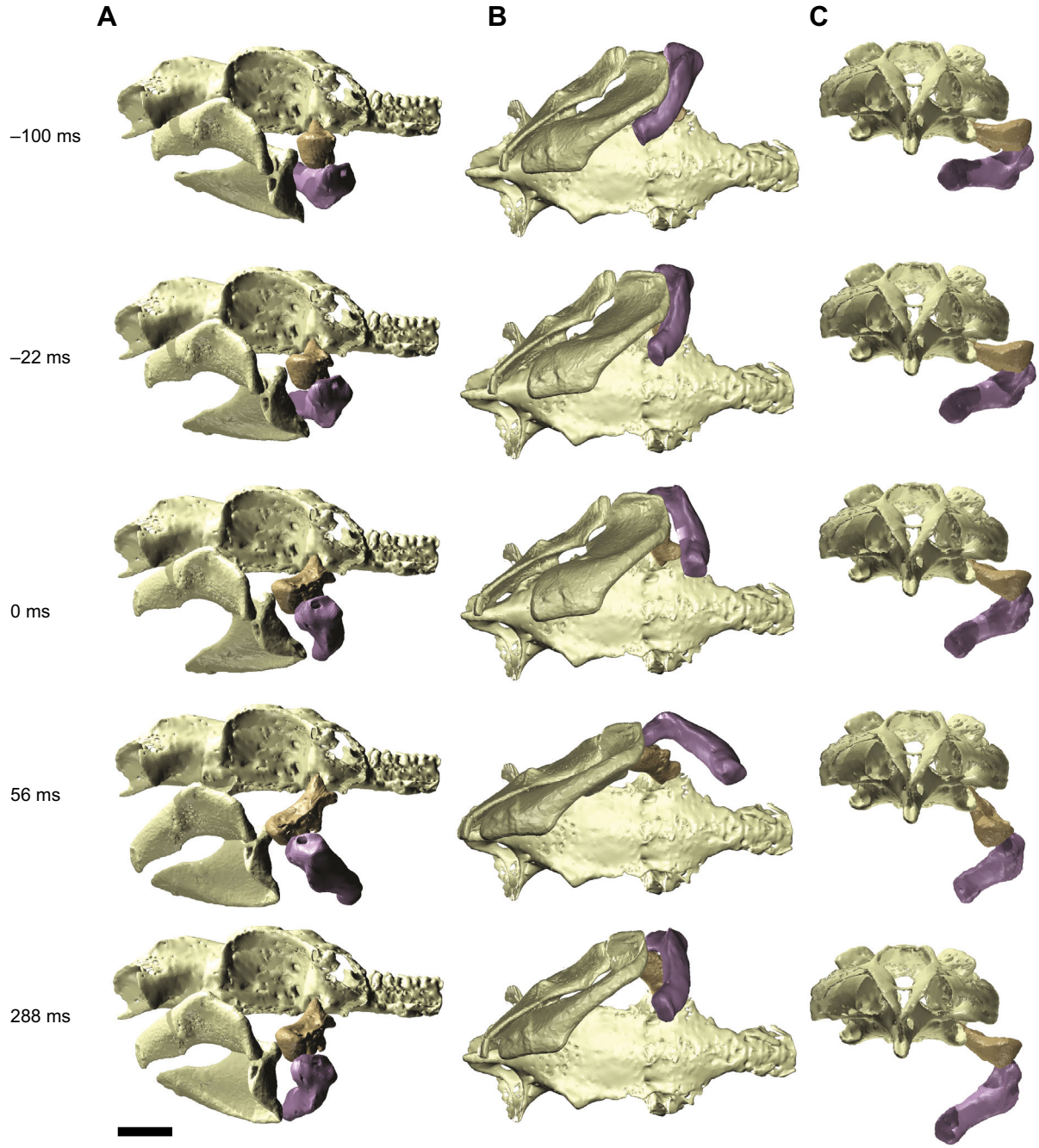

Fig. 4. Selected XROMM animation images from a typical suction capture event. Feeding sequence progresses from resting position (−100 ms), to peak gape (0 ms), to peak ceratohyal depression (56 ms) and then to recovery phase (56–288 ms). Left side elements only are shown, with hyomandibula (orange) and ceratohyal (purple) highlighted. Sequence is shown from (A) left lateral view, (B) ventral view, and (C) anterior view with upper and lower jaws removed. Note that most of the protraction of the hyomandibula and rostral protrusion of the upper jaw occurred before peak gape (−22 to 0 ms), whereas most of the medioventral hyomandibula motion and ventral protrusion of the upper jaw occurred after peak gape (0 to 56 ms). Scale bar: 10 mm.

Journal of Experimental Biology (2019) 222, jeb193573. doi:10.1242/jeb.193573

peak rotation. As the hyomandibula and ceratohyal continued to depress after peak gape, the distal end of the hyomandibula displaced medially, constricting the hyoid cavity as depression of the ceratohyal expanded the cavity ventrally (Fig. 4B,C between 0 and 56 ms). The distal end of the ceratohyal moved caudally as it depressed, retracting well past the hyomandibuloceratohyal joint (Fig. 4A,B at 56 ms). At the same time that the distal end of the ceratohyal retracted, the distal end of the hyomandibula and the proximal end of the ceratohyal protruded rostrally, pushing the jaws to their most protruded position at 56 ms. Retraction and depression of the ceratohyal and rotation of the hyomandibula peaked following peak gape (Fig. 4 at 56 ms), typically beginning the recovery just before the jaws were fully closed and continuing long after the jaws were closed (Fig. 4 at 288 ms).

Rotations of the hyomandibula and ceratohyal relative to the chondrocranium

Relative to the chondrocranium, the hyomandibula protracts, depresses and rotates about its long axis and the ceratohyal retracts, depresses and rotates about its long axis (Fig. 5). The hyomandibula and ceratohyal elements are nearly cylindrical, making it somewhat difficult to visualize LAR in the XROMM animations (Fig. 4; Movies 1 and 2 for the hyomandibula and ceratohyal; the red ball was digitally fixed to the dorsal edge of the element and motion in front of or behind the element indicates direction and extent of LAR). Data from the JCSs, however, showed substantial LAR in both elements (Fig. 5). The hyomandibula and ceratohyal rotated in opposite directions, with the dorsal margin of the hyomandibula moving rostrally and the dorsal margin of the ceratohyal moving caudally. The magnitude of LAR of the hyomandibula was greater than protraction and depression, with means (±s.e.m.) of −34.4±3.2, 29.8 ±1.9 and −28.2±3.6 degrees, respectively (Table 1). Initially, the dorsal margin of the ceratohyal rotated slightly rostrally, but then made a greater caudal rotation (Fig. 5B). Rostral LAR of the ceratohyal was small, −12.2±2.0 deg, and caudal LAR was greater, 31.3±3.8 deg, but smaller than retraction and depression at −43.4±2.0 and −47.0±4.4 deg, respectively.

All three rotations of the ceratohyal and hyomandibula peaked at about 50 ms after peak gape, but with a wide range of variation (Table 1). However, the proportion of rotation that occurs prior to and after peak gape differed between the two elements (Table 2). The hyomandibula was already substantially protracted by peak gape (65.3±3.5% of maximum protraction), but little depression occurred before peak gape (16.2±5.2% of maximum depression). By contrast, ceratohyal retraction (52.2±8.5% of maximum retraction) and depression (51.7±4.5% of maximum depression) occurred fairly equally before and after peak gape (Table 2).

Displacement of hyoid and mandibular arch landmarks

Rotations of the hyoid elements generated corresponding displacements of the distal ends of the ceratohyal and hyomandibula (Fig. 6A,B). Protraction of the hyomandibula (Fig. 5A, rotation about *y*-axis) resulted in a rostral displacement of the distal end of the hyomandibula (green trace, Fig. 6A) by a mean of 7.3±0.5 mm (Table 1). At the same time, depression moved the distal end of the hyomandibula −6.2±0.7 mm ventrally and 6.8±0.6 mm medially, constricting the buccal cavity as the distal end of the ceratohyal displaced −12.8±0.7 mm ventrally to expand the

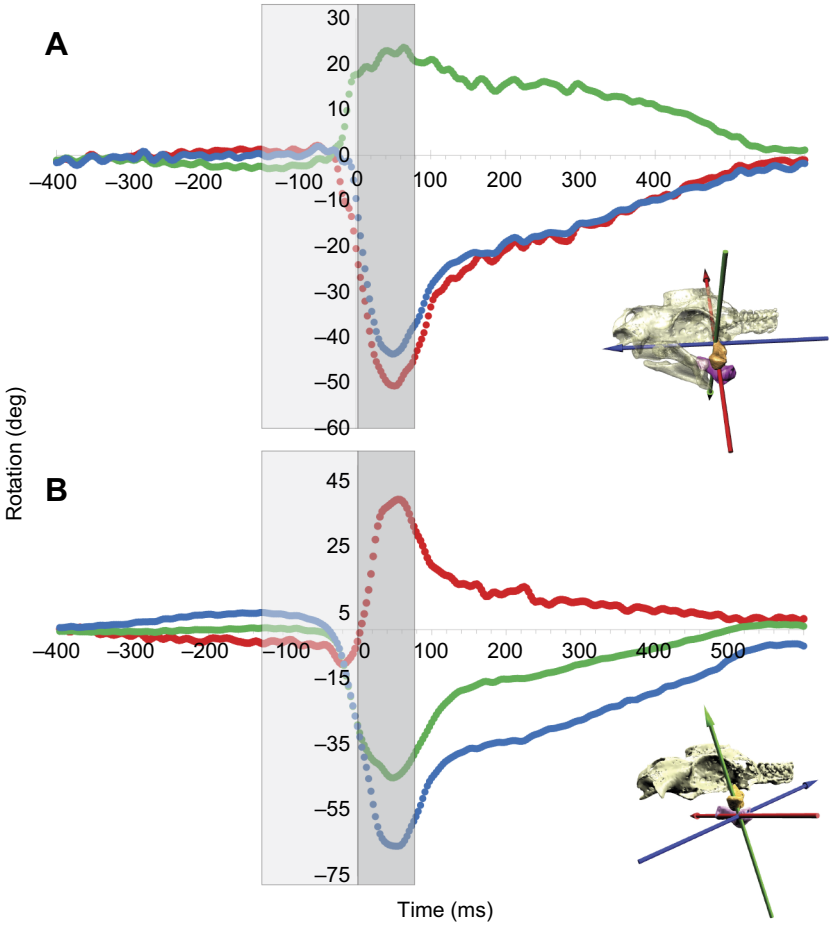

Fig. 5. Rotations of the hyomandibula and ceratohyal relative to the cranium. Results are shown for the same suction capture event as in Fig. 4 for (A) hyomandibula and (B) ceratohyal. Colors on the graphs correspond to rotation around the colored axes shown in the inset JCS images and Fig. 3, hyomandibula highlighted orange and ceratohyal in purple. Red is the *x*-axis, showing LAR. Green is the *y*-axis, showing protraction (positive) and retraction (negative), and blue is the *z*-axis, showing depression (negative). Light gray box shows mouth opening, dark gray shows mouth closing and peak gape occurs at time 0. For the hyomandibula, note the rapid and substantial protraction (green) prior to peak gape and prior to depression of the hyomandibula (blue). For both hyomandibula and ceratohyal, note the substantial LAR (red).

Journal of Experimental Biology (2019) 222, jeb193573. doi:10.1242/jeb.193573

Table 1. Mean magnitude and timing (in seconds relative to time of peak gape) of peak rotations (deg) and displacements (mm) of the hyomandibula and ceratohyal

	Rotation[a]			Displacement[b]	
	Mean	s.e.m.		Mean	s.e.m.
Hyomandibula timing					
Rostral LAR (*x*-axis)	54.3	1.24	Medial (*x*-axis)	47.9	3.69
Protraction (*y*-axis)	50.8	2.69	Rostral (*y*-axis)	49.0	4.66
Depression (*z*-axis)	59.6	5.55	Ventral (*z*-axis)	53.7	3.44
Hyomandibula magnitude					
Rostral LAR (*x*-axis)	−34.4	3.23	Medial (*x*-axis)	6.8	0.55
Protraction (*y*-axis)	29.8	1.92	Rostral (*y*-axis)	7.3	0.47
Depression (*z*-axis)	−28.2	3.62	Ventral (*z*-axis)	−6.2	0.66
Ceratohyal timing					
Rostral LAR (*x*-axis)	−6.7	5.40	–		
Caudal LAR (*x*-axis)	55.0[c]	2.08	Lateral (*x*-axis)	−60.1	45.24
Retraction (*y*-axis)	47.5	2.52	Caudal (*y*-axis)	48.3	2.21
Depression (*z*-axis)	50.8	1.34	Ventral (*z*-axis)	69.0	6.11
Ceratohyal magnitude					
Rostral LAR (*x*-axis)	−12.2	1.95	–		
Caudal LAR (*x*-axis)	31.3[c]	3.82	Lateral (*x*-axis)	−1.3	0.35
Retraction (*y*-axis)	−43.4	1.95	Caudal (*y*-axis)	−13.3	1.08
Depression (*z*-axis)	−47.0	4.42	Ventral (*z*-axis)	−12.8	0.74

LAR, long-axis rotation.
[a]Rotations of the hyomandibula and ceratohyal measured with JCSs shown in Fig. 3.
[b]Displacements of hyomandibular and ceratohyal landmarks shown in Fig. 6.
[c]Excluding 4 trials with no positive caudal LAR during strikes.

buccal cavity (Table 1). Ceratohyal rotation about the *y*-axis moved the distal end caudally by −13.3±1.1 mm. In the trial shown there is also lateral displacement of the distal end of the ceratohyal (Fig. 6B) that does not occur in all trials. The distal end of the hyomandibula begins protracting prior to peak gape, extending rostrally 5.3±0.4 mm by peak gape, which is 75% of maximum protraction (Table 2), but the distal end of the hyomandibula moves medially and ventrally later (only 41% and 32% of maximum magnitude by peak gape, respectively). Translation of the distal end of the ceratohyal closely follows the pattern in rotation, with approximately half the caudal and ventral translation occurring by peak gape (55% and 44%, respectively).

Table 2. Mean percentage of peak rotations and displacements reached by the time of peak gape

	Rotation (%)[a]	
	Mean	s.e.m.
Hyomandibula		
Rostral LAR (*x*-axis)	42	5.0
Protraction (*y*-axis)	65	3.5
Depression (*z*-axis)	16	5.2
Ceratohyal		
Retraction (*y*-axis)	52	8.5
Depression (*z*-axis)	52	4.5
	Displacement (%)[b]	
	Mean	s.e.m.
Hyomandibula		
Medial (*x*-axis)	41	5.8
Rostral (*y*-axis)	75	4.4
Ventral (*z*-axis)	32	6.9
Ceratohyal		
Caudal (*y*-axis)	55	4.7
Ventral (*z*-axis)	44	5.0

[a]Rotations of the hyomandibula and ceratohyal measured with JCSs shown in Fig. 3.
[b]Displacements of hyomandibular and ceratohyal landmarks shown in Fig. 6.

Protraction and depression of the distal end of the hyomandibula results in a displacement of the jaw joint (Motta and Wilga, 1999) and the tips of the jaws. The jaw joint displacement peaks at 4.6±0.2 mm rostrally and −6.4±0.4 mm ventrally, at 49.5±2.9 ms and 44.1±4.1 ms after peak gape, respectively, while the tip of the upper jaw moves 5.0±0.3 mm rostrally and −13.5±1.2 mm ventrally as the upper jaw depresses (28.0±4.8 ms and 50.9±4.9 ms after peak gape, again respectively). More importantly, the upper jaw begins to protrude prior to peak gape, reaching 3.8±0.3 mm by peak gape, which is 75% of maximum rostral displacement and an average of 5.9% of the length of the cranium (e.g. Fig. 4A). Depression of the upper jaw begins later in the feeding cycle, with the tip only reaching 23% of maximum ventral displacement by peak gape.

Regressions

At peak gape, standardized major axis regression showed ceratohyal depression had a close relationship with LAR and with retraction (Fig. 7A,C). Hyomandibula LAR and depression also had a close relationship (Fig. 7B); however, depression of the hyomandibula showed no significant relationship with protraction (Fig. 7D).

Standardized major axis regression comparing peak motions, rather than motion by the time of peak gape, showed no significant relationship between the peak magnitudes of retraction of the ceratohyal and ceratohyal depression (Fig. 7G). A strong relationship exists between magnitude of ceratohyal LAR and ceratohyal depression (Fig. 7E). Hyomandibula LAR varied strongly with hyomandibula depression (Fig. 7F), while protraction showed no significant relationship with hyomandibula depression (Fig. 7H). Depression of the ceratohyal was smaller in trials with no positive LAR (mean −30 deg) compared to trials with a positive peak in LAR (mean −45 deg, $P<0.0001$).

DISCUSSION

Bamboo sharks are high-performance suction feeders that also show non-stereotyped feeding strikes (*sensu* Wainwright et al., 2008) and are considered to be functional generalists (*sensu* Wilga

Journal of Experimental Biology (2019) 222, jeb193573. doi:10.1242/jeb.193573

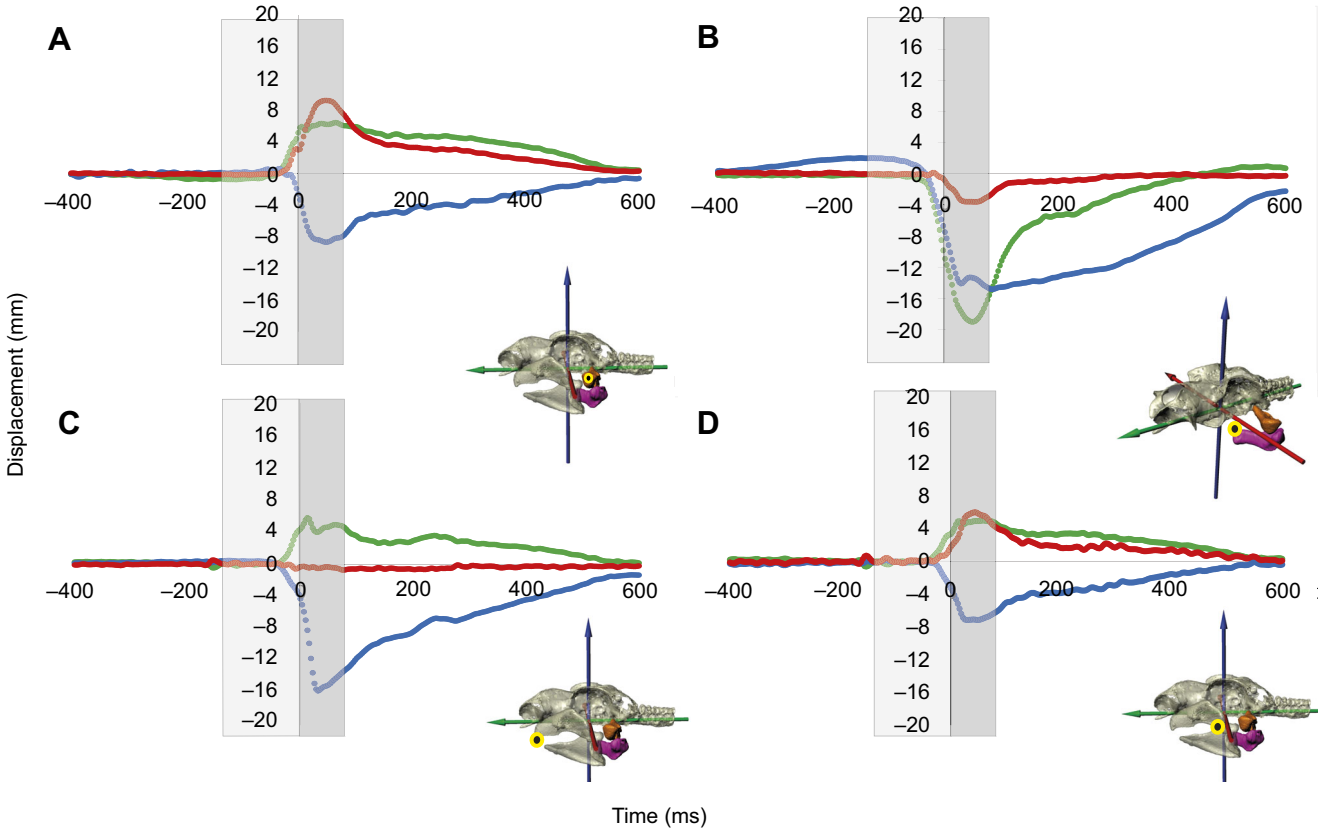

Fig. 6. Displacement of landmarks on the hyomandibula, ceratohyal and palatoquadrate relative to a cranial anatomical coordinate system (ACS). Insets show the ACS, and the yellow and black circles show the landmarks tracked. Hyomandibula is highlighted orange, ceratohyal is purple in each inset. (A) Displacement of the distal end of the hyomandibula. (B) Displacement of the distal end of the ceratohyal. (C) Displacement of the rostral tip of palatoquadrate. (D) Displacement of the medial quadratomandibular joint facet on palatoquadrate. The ACS is oriented such that displacement along the red (*x*-axis) is medial (positive) and lateral (negative), green (*y*-axis) is rostral (positive) and caudal (negative), and blue (*z*-axis) is dorsal (positive) and ventral (negative).

et al., 2012). High suction performance likely results from strong, fast and precisely coordinated motions of the hyoid and mandibular arches, but until now these motions could not be visualized directly because of the thick skin and labial cartilages obscuring the hyomandibula, ceratohyal and jaws. We used XROMM to test, and largely to confirm, prior hypotheses for the 3D motions of these elements based on external video, sonomicrometry and *ex vivo* manipulations (Wu, 1994; Wilga and Sanford, 2008; Ramsay, 2012; Ramsay and Wilga, 2017).

Protraction and retraction of the hyoid elements

Two motions of the hyoid elements act to expand the hyoid region of the oral cavity while suction feeding: the distal end of the hyomandibula rotates rostrally (protracts), lengthening the hyoid region, and the distal end of the ceratohyal retracts, enlarging the depth. Ceratohyal retraction and hyomandibula protraction peak at nearly the same time that they depress after peak gape (Table 1). The ceratohyal retracts past the hyomandibuloceratohyal and craniohyomandibular joints, the long axis swinging from rostral horizontal, to vertical, to well beyond a vertical position (Fig. 4A, compare −100 ms with 56 ms). Owing to their common linkage at the hyomandibuloceratohyal joint, retraction and depression of the ceratohyal induces a remarkable degree of protraction and depression of the hyomandibula. Protraction of the hyomandibula, in turn, pushes the jaws rostrally (Fig. 4; Wu, 1994; Ramsay, 2012).

Although it is clear that the large rotations of the hyomandibula and ceratohyal drive suction performance in bamboo sharks, a paradox of these motions is that they cause a decrease in buccal cavity width while increasing depth and length (Wilga, 2008; Wilga and Sanford, 2008). This medial compression is caused by the protraction and depression of the hyomandibula causing medial displacement of the distal tip of the hyomandibula (Fig. 6A). We found with XROMM that less than half of the medial displacement of the tip of the hyomandibula occurs by peak gape (Fig. 5 and Table 2), thereby mitigating the effect of this paradoxical motion.

Protraction and retraction of the hyoid arch transforms the shape of the oral cavity by lengthening the buccal cavity relative to ventral expansion. Voluntarily varying the shape of the oral cavity may enable individual sharks to alter pressure profiles or shift the time of peak pressure among strikes depending on the strike tactic. The timing and magnitude of peak pressure during strikes can vary greatly within individual white-spotted bamboo sharks, characterizing them as functional generalists (Wilga and Sanford, 2008; Wilga et al., 2012). Mechanistic variation allows bamboo sharks to adjust their highly specialized feeding strategy for a wide variety of prey types, prey positions or hunting substrate (Compagno, 1984; Nauwelaerts et al., 2007; Wilga et al., 2007, 2012). The area of fluid ingested was 56% larger in successful strikes compared with unsuccessful strikes in suction feeding bamboo sharks (Nauwelaerts et al., 2008). The durations were similar and the period too short for feedback control, which suggests that motivation or distance from the prey were factors (Nauwelaerts et al., 2008). These significant changes in pressure among strikes in

Journal of Experimental Biology (2019) 222, jeb193573. doi:10.1242/jeb.193573

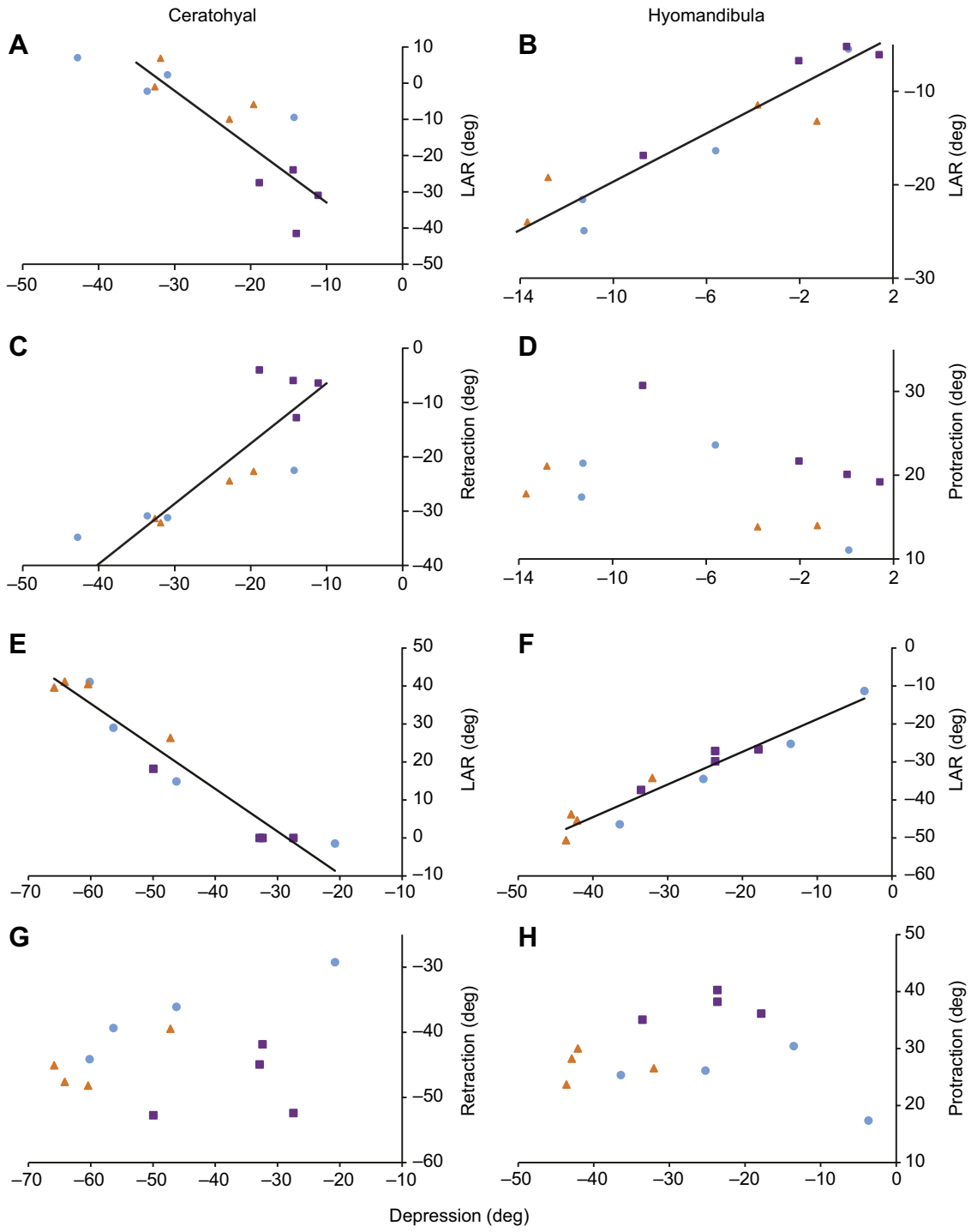

Fig. 7. Standardized major axis regressions for rotations of the ceratohyal and hyomandibula at peak gape (A–D) and peak rotation (E–H). (A) Ceratohyal LAR versus depression at peak gape (R^2=0.69, coefficient=−1.57, P<0.001). (B) Hyomandibula LAR versus depression at peak gape (R^2=0.88, coefficient=1.32, P<0.001). (C) Ceratohyal retraction versus depression at peak gape (R^2=0.72, coefficient=1.13, P<0.001). (D) Hyomandibula retraction versus depression at peak gape (no significant regression; P=0.93). (E) Peak ceratohyal LAR versus depression (R^2=0.92; coefficient=−1.15; P<0.001). (F) Peak hyomandibula LAR versus depression (R^2=0.93; coefficient=0.89; P<0.001). (G) Peak ceratohyal retraction versus depression (no significant regression; P=0.304). (H) Peak hyomandibula retraction versus depression (no significant regression; P=0.95). Orange triangle, shark Bam02; blue circle, shark Bam03; and purple square, shark Bam04.

bamboo sharks may be produced by changes in the shape of the oral chamber (Van Wassenbergh et al., 2006; Nauwelaerts et al., 2008).

Bamboo sharks may vary timing and magnitude of suction pressure among strikes by decoupling the magnitude of protraction/retraction from depression in the expansion mechanism (Nauwelaerts et al., 2008; Wilga et al., 2012). We found that the magnitude of hyomandibular protraction varies independently of depression and LAR during prey capture (Fig. 7D,H). While protraction and retraction of the hyoid elements peak at nearly the same time as depression and LAR (Fig. 5), the magnitude of protraction can vary

Journal of Experimental Biology (2019) 222, jeb193573. doi:10.1242/jeb.193573

considerably independently of hyoid depression, increasing flexibility and variability in the suction mechanism of bamboo sharks compared with other, more stereotyped suction-feeding vertebrates (Fig. 7; Wilga et al., 2012). In other words, the amount of depression does not affect the amount of protraction, despite peak rotations occurring close in time during feeding. Ceratohyal retraction occurs with depression until peak gape then decouples afterwards, possibly to accommodate the influx of water following prey capture.

Jaw protrusion in bamboo sharks

The tip of the upper jaw began protruding rostrally prior to peak gape (Fig. 4; Fig. 5A). Rostral rotation of the hyoid arch pushes the jaws forward, thereby increasing the anterior volume of the oral cavity, which is convergent with upper jaw protrusion in teleosts. Protrusion of the jaws in elasmobranchs typically follows prey capture and peaks around jaw closure (Frazzetta and Prange, 1987; Moss, 1972; Motta et al., 2008; although see Sasko et al., 2006 for an exception). In bamboo sharks, early forward protrusion by the upper jaw is obscured by labial folds covering the lateral sides of the gape in light-cinematography based analyses. While ventral jaw motion is still much greater than the forward motion, and peaks later in a strike as in other shark species (Edmonds et al., 2001; Motta et al., 2008; Wilga and Motta, 1998), the majority of forward motion of the upper jaw has taken place by peak gape in bamboo sharks (75% of peak rostral displacement; Fig. 4 and Fig. 6C). By increasing oral cavity volume, as well as moving the mouth forward relative to the head, jaw protrusion can increase rate of flow into the mouth (Holzman et al., 2008). Thus, protrusion in bamboo sharks is similar to that in teleost fishes, and likely enhances suction forces at the mouth (Holzman et al., 2008). Combined with protraction of the hyomandibula, jaw protraction could enhance the impact of decoupling protraction and depression on altering flow and pressure during feeding. Future research focusing on the suction performance of elasmobranchs that incorporates three-dimensional kinematic reconstruction of the hyoid elements should quantify changes in oral volume and *in vivo* measurements of pressure, as has been done in teleosts (Camp et al., 2015) to address the effect of hyoid protraction and retraction on suction performance in suction-feeding shark species.

Long-axis rotation

Substantial LAR of the hyomandibula and ceratohyal was revealed using XROMM, a phenomenon that previously was not visible in the feeding apparatus of vertebrates using conventional methods. Based on this study, LAR of hyoid elements may be a key component in expanding and compressing the oral cavity to generate suction in elasmobranchs. LAR has been proposed for the upper and lower jaws (Frazzetta and Prange, 1987; Ramsay and Wilga, 2007) of sharks, and in the lower jaw of anteaters (Naples, 1999) during feeding. However, prior to this study, *in vivo* measurements of LAR of skeletal elements have only been made in the lower jaws of some mammals (e.g. Lieberman and Crompton, 2000) and from studies of the limbs and girdles of ground-walking birds and turtles (Kambic et al., 2014; Mayerl et al., 2016).

The direction of rotation may relate to articulation of the hyoid elements at their proximal and distal joints during depression, similar to the rotation within the mandible of some teleost fishes that maintains proper articulation of quadratomandibular joints and the mandibular symphysis during jaw depression (Aerts, 1985). In bamboo sharks, the hyoid elements rotate in the same direction (dorsal margin rotating rostrally) around their long axes during the expansion phase; however, as the ceratohyal depresses, the direction of LAR changes and the dorsal margin rotates caudally (Figs 5 and 8). The hyomandibula has two articulation facets with the cranium at its proximal end (see Motta and Wilga, 1999 for a detailed description of cranial articulations). Forward rotation of the dorsal margin may keep the rostral and caudal craniohyomandibular condyles articulated with the cranium throughout depression. Without LAR, the proximal end of the hyomandibula might disarticulate from the cranium at higher degrees of depression. Similarly to the hyomandibula, the ceratohyal may rotate around its long axis to maintain articulation with the hyomandibula at its proximal end and basihyal at its distal end. Unfortunately, we did not mark the basihyal for this study, so we could not animate it. However, the anatomy of the joint between the ceratohyal and the basihyal suggests that ceratohyal LAR may help keep this joint articulated. The distal end of the ceratohyal is triangular with a caudal–dorsal lobe that fits under a caudal shelf on the basihyal when the hyoid is in resting position. Rostral LAR of the ceratohyal may tilt the basihyal forward during the initial expansion. Further depression may slide the distal end of the ceratohyal forward along the basihyal, the caudal–dorsal lobe of the ceratohyal rotating under the basihyal through caudal LAR.

Although LAR timed closely with protraction and depression of the hyomandibula and ceratohyal, only the magnitude of depression showed a strong relationship with the magnitude of LAR (Fig. 7). Ceratohyal LAR, though less extreme (Table 1), is more variable, likely because of the looser ligamentous connection to the distal end of the hyomandibula (Motta and Wilga, 1999; Ramsay and Wilga, 2017). While the ceratohyal still depresses in the absence of caudal LAR, depression is stronger when LAR is predominantly caudal. Feeding attempts with only negative (dorsal margin rotates rostrally) LAR also had lower magnitudes of depression than those attempts with only positive (dorsal margin rotates caudally) LAR, but were still sufficient for a successful strike. The impact of this difference in

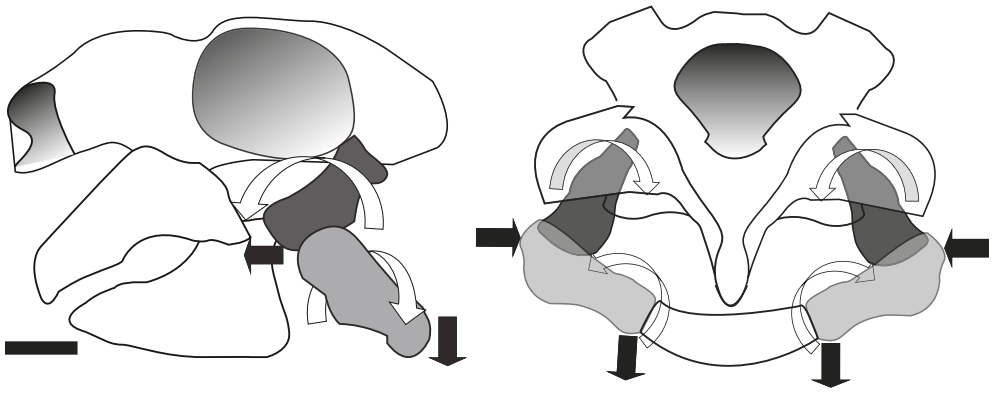

Fig. 8. LAR of the hyomandibula and the ceratohyal following peak gape. Lateral view (left) and anterior view (right) of hyomandibula (dark gray) and the ceratohyal (light gray). Black arrows show the motions of the hyomandibula and the ceratohyal. White arrows show direction of LAR of the hyomandibula and ceratohyal. Here the ceratohyal is fully depressed, corresponding to the 56 ms row in Fig. 4. Scale bar: 10 mm.

LAR on suction performance (pressure, flow, accuracy) remains unknown, but reduced depression could reduce volume change and therefore pressure and rate of flow.

LAR may also have broad implications for load and force distribution among elements during suction capture events. LAR may transmit compressive or tensile forces from the load bearing elements through the ligamentous connections to other elements (Motta and Wilga, 1999; Ramsay and Wilga, 2017), thus distributing the load throughout the feeding apparatus. The hyomandibula of bamboo sharks is stiffer than that in non-suction-feeding sharks, and is capable of bearing considerable load with less strain (Balaban et al., 2015). LAR of the ceratohyal may transfer forces from the hyoid depressor muscles (coracohyoideus and coracoarcualis; Motta and Wilga, 1999; Motta et al., 2008; Ramsay and Wilga, 2017) to the hyomandibula, which, in turn, distributes force to the cranium. If LAR is related to reducing or redistributing force, then it may be less prevalent in the hyoid kinematics of non-suction-feeding shark species, where the hyoid arch may be under less stress.

Concluding remarks

Bamboo sharks are high-performance suction feeders that expand oral volume and shape the oral cavity using complex combinations of hyoid rotations. XROMM confirms remarkably large rotation arcs of both the hyomandibula and ceratohyal and shows, for the first time, extensive LAR of these elements. These large LARs may increase the range of motion possible during ventral expansion of the oral cavity, a major contributor to high-performance suction in this species. XROMM also demonstrated decoupling of the magnitude of ventral expansion from forward and backward motions of the hyoid elements, which may extend the range of suction performance possible by modulating the shape of the oral cavity during feeding. Such a mechanism could allow bamboo sharks to obtain a varied diet, despite the physical constraints of generating suction with a limited number of skeletal elements. Early protraction of the hyomandibula also drives forward upper jaw protrusion during prey capture; the same mechanism used by teleost fishes to increase oral volume and flow rate at the mouth. Hence, suction feeding in bamboo sharks is convergent with many aspects of suction feeding in ray-finned fishes, including early jaw protrusion, but hyoid rotations are more extreme than in most ray-finned fishes, likely facilitated by the extra degrees of freedom in the hyostylic jaw suspension system and large LAR of the paired hyoid elements.

Acknowledgements

The authors would like to thank Erika Tavares for aid setting up and running XROMM trials, Ben Knörlein for contribution of software and expertise to computer analysis of marker tracking, David Baier for the XROMM MayaTools, Ben Concepcion and Laura Vigil for care and training of bamboo sharks used in the trials and Nicholas Gidmark for advice on rendering and presenting images from Maya.

Competing interests

The authors declare no competing or financial interests.

Author contributions

Conceptualization: C.A.D.W., E.L.B.; Methodology: E.L.B.; Formal analysis: B.S., E.L.B.; Investigation: B.S., C.A.D.W., E.L.B.; Data curation: B.S., C.A.D.W., E.L.B.; Writing - original draft: B.S., C.A.D.W., E.L.B.; Writing - review & editing: B.S., C.A.D.W., E.L.B.; Visualization: B.S.; Supervision: C.A.D.W., E.L.B.

Funding

Funding was provided by the U.S. National Science Foundation (IOS-1354189 to C.A.D.W. and DBI-1661129 and IOS-1655756 to E.L.B.), as well as Graduate Teaching Assistantships from the University of Rhode Island.

Data availability

Data for this publication have been deposited and opened for public use in the XMAPortal (xmaportal.org), in the study 'Bamboo Shark Feeding' with the permanent identifier URI1.

Supplementary information

Supplementary information available online at
http://jeb.biologists.org/lookup/doi/10.1242/jeb.193573.supplemental

References

Aerts, P. (1985). The intramandibular linkage in *Astatotilapia elegans* (Teleostei, Cichlidae): appearance and function of the Meckelian cartilage. *J. Zool.* **205**, 391-410.

Alexander, R. M. N. (1967). The functions and mechanisms of the protrusible upper jaws of some acanthopterygian fish. *J. Zool.* **151**, 43-64.

Balaban, J. P., Summers, A. P. and Wilga, C. A. (2015). Mechanical properties of the hyomandibula in four shark species. *J. Exp. Zool. A* **323**, 1-9.

Brainerd, E. L., Baier, D. B., Gatesy, S. M., Hedrick, T. L., Metzger, K. A., Gilbert, S. L. and Crisco, J. J. (2010). X-ray reconstruction of moving morphology (XROMM): precision, accuracy and applications in comparative biomechanics research. *J. Exp. Zool. A* **313A**, 262-279.

Brainerd, E. L., Blob, R. W., Hedrick, T. L., Creamer, A. T. and Müller, U. K. (2017). Data management rubric for video data in organismal biology. *Integr. Comp. Biol.* **57**, 33-47.

Camp, A. L. and Brainerd, E. L. (2015). Reevaluating musculoskeletal linkages in suction feeding fishes with X-ray Reconstruction of Moving Morphology (XROMM). *Integr. Comp. Biol.* **55**, 1-12.

Camp, A. L., Roberts, T. J. and Brainerd, E. L. (2015). Swimming muscles power feeding in largemouth bass. *Proc. Natl. Acad. Sci. USA* **112**, 8690-8695.

Camp, A. L., Scott, B., Brainerd, E. L. and Wilga, C. D. (2017). Dual function of the pectoral girdle for feeding and locomotion in white-spotted bamboo sharks. *Proc. Biol. Sci.* **284**, 20170847.

Camp, A. L., Roberts, T. J. and Brainerd, E. L. (2018). Bluegill sunfish use high power outputs from axial muscles to generate powerful suction-feeding strikes. *J. Exp. Biol.* **221**, jeb178160.

Compagno, L. J. V. (1984). Sharks of the World. *FAO Fish Synopsis No. 125* **4**, 1-655.

Edmonds, M. A., Motta, P. J. and Hueter, R. E. (2001). Food capture kinematics of the suction feeding horn shark, *Heterodontus francisci*. *Environ. Biol. Fish* **62**, 415-427.

Frazzetta, T. H. and Prange, C. D. (1987). Movements of cephalic components during feeding in some requiem sharks (Carcharhiniformes: Carcharhinidae). *Copeia* **1987**, 979-993.

Gidmark, N. J., Staab, K. L., Brainerd, E. L. and Hernandez, L. P. (2012). Flexibility in starting posture drives flexibility in kinematic behavior of the kinethmoid mediated premaxillary protraction mechanism in a cyprinid fish, *Cyprinus carpio*. *J. Exp. Biol.* **215**, 2262-2272.

Holzman, R., Day, S. W., Mehta, R. S. and Wainwright, P. C. (2008). Jaw protraction enhances suction forces exerted on prey by suction feeding fishes. *J. R. Soc. Interface* **5**, 1445-1457.

Kambic, R. E., Roberts, T. J. and Gatesy, S. M. (2014). Long-axis rotation: a missing degree of freedom in avian bipedal locomotion. *J. Exp. Biol.* **217**, 2770-2782.

Knörlein, B. J., Baier, D. B., Gatesy, S. M., Laurence-Chasen, J. D. and Brainerd, E. L. (2016). Validation of XMALab software for marker-based XROMM. *J. Exp. Biol.* **219**, 3701-3711.

Lieberman, D. E. and Crompton, A. W. (2000). Why fuse the mandibular symphysis? A comparative analysis. *Am. J. Phys. Anthropol.* **112**, 517-540.

Liem, K. F. (1967). Functional morphology of the head of the anabantoid teleost fish *Helostoma temmincki*. *J. Morphol.* **121**, 135-157.

Mayerl, C. J., Brainerd, E. L. and Blob, R. W. (2016). Pelvic girdle mobility of cryptodire and pleurodire turtles during walking and swimming. *J. Exp. Biol.* **219**, 2650-2658.

Menegaz, R. A., Baier, D. B., Metzger, K. A., Herring, S. W. and Brainerd, E. L. (2015). XROMM analysis of tooth occlusion and temporomandibular joint kinematics during feeding in juvenile miniature pigs. *J. Exp. Biol.* **218**, 2573-2584.

Moss, S. A. (1972). The feeding mechanism of sharks of the family Carcharhinidae. *Proc. Zool. Soc.* **167**, 423-436.

Motta, P. J. and Wilga, C. D. (1999). Anatomy of the feeding apparatus of the nurse shark, *Ginglyostoma cirratum*. *J. Morphol.* **241**, 33-60.

Motta, P. J., Hueter, R. E., Tricas, T. C., Summers, A. P., Huber, D. R., Lowry, D., Mara, K. R., Matott, M. P., Whitenack, L. B. and Wintzer, A. P. (2008). Functional morphology of the feeding apparatus, feeding constraints and suction performance in the nurse shark *Ginglyostoma cirratum*. *J. Morphol.* **269**, 1041-1055.

Naples, V. L. (1999). Morphology, evolution and function of feeding in the giant anteater (*Myrmecophaga tridactyla*). *J. Zool. Lond.* **249**, 19-41.

Nauwelaerts, S., Wilga, C. D., Sanford, C. P. and Lauder, G. V. (2007). Hydrodynamics of prey capture in sharks: effects of substrate. *J. R. Soc. Interface* **4**, 341-345.

Nauwelaerts, S., Wilga, C. D., Lauder, G. V. and Sanford, C. P. (2008). Fluid dynamics of feeding behavior in white spotted bamboo sharks. *J. Exp. Biol.* **211**, 3095-3102.
Olsen, A. M., Camp, A. L. and Brainerd, E. L. (2017). The opercular mouth-opening mechanism of largemouth bass functions as a 3D four-bar linkage with three degrees of freedom. *J. Exp. Biol.* **220**, 4612-4623.
Osse, J. W. M. (1969). Functional morphology of the head of a perch (*Perca fluviatilis L.*): An electromyographic study. *Neth. J. Zool.* **19**, 289-392.
Ramsay, J. B. (2012). A comparative investigation of cranial morphology, mechanics, and muscle function in suction and bite feeding sharks. *PhD Thesis. University of Rhode Island.* http://digitalcommons.uri.edu/dissertations/AAI3526224.
Ramsay, J. B. and Wilga, C. D. (2007). Morphology and Mechanics of the teeth and jaws of white-spotted bamboo sharks (*Chiloscyllium plagiosum*). *J. Morphol.* **268**, 664-682.
Ramsay, J. B. and Wilga, C. D. (2017). Function of the hypobranchial muscles and hyoidiomandibular ligament during suction capture and bite processing in white-spotted bamboo sharks, *Chiloscyllium plagiosum*. *J. Exp. Biol.* **220**, 4047-4059.
Sasko, D. E., Dean, M. N., Motta, P. J. and Hueter, R. E. (2006). Prey capture behavior and kinematics of the Atlantic cownose ray, *Rhinoptera bonasus*. *Zoology* **109**, 171-181.
Smith, R. J. (2009). Use and misuse of the reduced major axis for line-fitting. *Am. J. Phys. Anthropol.* **140**, 479-486.
Tchernavin, V. (1948). On the mechanical working of the head of bony fishes. *J. Zool.* **118**, 129-143.
Van Dobben, W. H. (1937). Über den Kiefermechanismus der Knochenfische. *Arch. Neerl. Zool.* **2**, 1-72.
Van Wassenbergh, S., Aerts, P. and Herrel, A. P. (2006). Hydrodynamic Modelling of aquatic suction performance and intra-oral pressures: limitations for comparative studies. *J. R. Soc. Interface* **2006**, 507-514.
Van Wassenberg, S., Strother, J. A., Flammang, B. E., Ferry-Graham, L. A. and Aerts, P. (2008). Extremely fast prey capture in pipefish is powered by elastic recoil. *J. R. Soc. Interface* **5**, 285-296.
Van Wassenbergh, S., Leysen, H., Adriaens, D. and Aerts, P. (2013). Mechanics of snout expansion in suction-feeding seahorses: musculoskeletal force transmission. *J. Exp. Biol.* **216**, 407-417.
Wainwright, P. C., Mehta, R. S. and Higham, T. E. (2008). Stereotypy, flexibility and coordination: central concepts in behavioral functional morphology. *J. Exp. Biol.* **211**, 3523-3528.
Wainwright, P. C., McGee, M. D., Longo, S. J. and Hernandez, L. P. (2015). Origins, innovations, and diversification of suction feeding in vertebrates. *Integr. Comp. Biol* **55**, 134-145.
Warton, D. I., Wright, I. J., Falster, D. S. and Westoby, M. (2006). Bivariate line-fitting methods for allometry. *Biol. Rev.* **81**, 259-291.
Welch, B. L. (1947). The generalization of 'Student's' problem when several different population variances are involved. *Biometrika* **34**, 28-35.
Wilga, C. D. (2008). Evolutionary divergence in the feeding mechanism of fishes. *Acta Geol. Pol.* **58**, 113-120.
Wilga, C. D. and Motta, P. J. (1998). Feeding mechanism of the Atlantic guitarfish *Rhinobatos lentiginosus*: modulation of kinematic and motor activity. *J. Exp. Biol.* **201**, 3167-3184.
Wilga, C. D. and Sanford, C. P. (2008). Suction generation in white-spotted bamboo sharks *Chiloscyllium plagiosum*. *J. Exp. Biol.* **211**, 3128-3138.
Wilga, C. A. D., Motta, P. J. and Sanford, C. P. (2007). Evolution and ecology of feeding in elasmobranchs. *Integr. Comp. Biol* **47**, 55-69.
Wilga, C. A. D., Stoehr, A. A., Duquette, D. C. and Allen, R. M. (2012). Functional ecology of feeding in elasmobranchs. *Environ. Biol. Fish* **95**, 155-167.
Wu, E. H. (1994). Kinematic analysis of jaw protraction in orectolobiform sharks: a new mechanism for jaw protraction in elasmobranchs. *J. Morphol.* **222**, 175-190.